Title: Analysis of resistive switching processes in TiN/Ti/HfO_2/W devices to mimic electronic synapses in neuromorphic circuits

Authors: G. González-Cordero[1], M. Pedro[2], J. Martin-Martinez[2], M.B. González[3], F. Jiménez-Molinos[1], F. Campabadal[3], N. Nafría[2], J.B. Roldán[1]

Address:

[1]Departamento de Electrónica y Tecnología de Computadores. Universidad de Granada. Facultad de Ciencias. Avd. Fuentenueva s/n, 18071 GRANADA, Spain. Email: jroldan@ugr.es

[2]Dept. Enginyeria Electrònica. Universitat Autònoma de Barcelona, Edifici Q. 08193 Bellaterra, Spain

[3]Institut de Microelectrònica de Barcelona, IMB-CNM (CSIC), Campus UAB, 08193 Bellaterra, Spain

Abstract:

The potential of resistive switching (RS) devices based on TiN/Ti/HfO_2/W stacks to mimic synapses within a neuromorphic applications context is analyzed in depth. The fabrication and characterization process are explained and a physically-based modeling description is performed to understand the devices resistive switching operation and conductance modulation. The model employed considers truncated-cone shaped conductive filament (CF) geometries and parasitic ohmic resistances linked to the device conductive filaments in addition to device capacitances. The temporal evolution is analysed assuming a valence change memory operation, where the oxide surrounding the CF is considered as well as the CF thermal description. A complete series of RS cycles has been fitted with the model by means of the gradient descent algorithm to study the compliance current effects on the conductance modulation. To do so, experimental and modeled results are extensively compared.

Index Terms — Conductive filaments, Neuromorphic applications, Parameter extraction, Physical model, Resistive switching memory, RRAM.

I.-INTRODUCTION

RRAM technology has been proved to be suitable for the implementation of electronic synapses in a neuromorphic architecture, because of its non-volatile memory properties, the analog control of its conductivity state, scalability and compatibility with CMOS technology [1-3]. Moreover, its device-level variability, which is a well-known issue in these devices [4, 5], could be mitigated by the learning algorithms employed in artificial neural networks, leading to a system with high resilience to device variability. In order to optimize the device operating point, electrical characterization and further modeling is needed to understand the underlying mechanisms of resistive switching (RS) phenomena. RS mastering is one of the keys for the implementation of an electronic synapse, where, analog control of the conductance is required to imitate the potentiation and depression processes that take place in the connections between neurons [3, 6]. This analog control allows to build a stronger or weaker link between neuronal circuits, mimicking the variation of the synaptic weight, i.e., the connection strength between neurons.

In this context, the use of simulations at both device and system-level can be essential to deepen on the physics behind RS and the operation of circuits based on RS devices. The information obtained by means of simulators can be used to explore the capabilities of RRAM technology for neuromorphic applications [3]. In this respect, we make use in this work of a previously developed RRAM physically-based model [7, 8] to characterize the device operation as synapses within a neuromorphic hardware

landscape where electronic circuits are thought to be employed in neuro-inspired computing. This compact model, once its capacity to work correctly by reproducing the behavior and main characteristics of the studied devices as electronic synapsis is proved, could be used in the future to aid the design of new neuromorphic circuits based on the technology presented here.

The model employed here has been previously described and validated [7-9] and includes important physical effects involved in the RS operation of the devices under consideration [7, 8]. Thermal effects and quantum mechanical effects, such as tunneling currents, are included along with redox reactions to control the dynamics of CF rupture and rejuvenation [5, 7, 9, 10-13]. Parasitic effects such as series resistances and capacitances are also incorporated in the physical description. In addition, the model, in a compact form, has been implemented in circuit simulators [7, 9] with the purpose of analyzing RS cycles with a fixed compliance current. In this work, RS cycles under variable compliance currents are experimentally obtained and analyzed with our model in order to characterize TiN/Ti/HfO_2/W devices. We have studied the possibilities to modulate the device conductance state by means of the compliance current and assess the devices potential to be employed as electronic synapses.

The fabrication technology and measurement details are explained in section II, the model main features are described in section III and results and discussion are given in section IV. Finally, we extract the main conclusions in section V.

II.-DEVICE DESCRIPTION AND MEASUREMENT SET-UP

The devices employed in this study are TiN/Ti/HfO_2/W Metal-Insulator-Metal (MIM) structures in a single device cross-bar configuration and an area of 5 × 5 μm^2 (see Figure 1) [7, 8]. They were fabricated on 100 mm-diameter Si wafers. The fabrication process started with a thermal oxidation, leading to a 200 nm SiO_2 layer to isolate the MIM devices from the Si substrate. Next, the bottom electrode, consisting of a 200 nm-thick W layer was deposited by magnetron sputtering and patterned by photolithography and dry etching. Then, a 10 nm HfO_2 insulator layer was deposited by atomic layer deposition (ALD) at 225 °C using TDMAH and H_2O as precursors and N_2 as carrier and purge gas. After the ALD process, the top electrode, consisting of 200nm TiN and 10nm Ti, was deposited by magnetron sputtering and patterned by photolithography and dry etching. Finally, the contact area to the bottom electrode was defined by photolithography and dry etching of the HfO_2 film on top of the W layer.

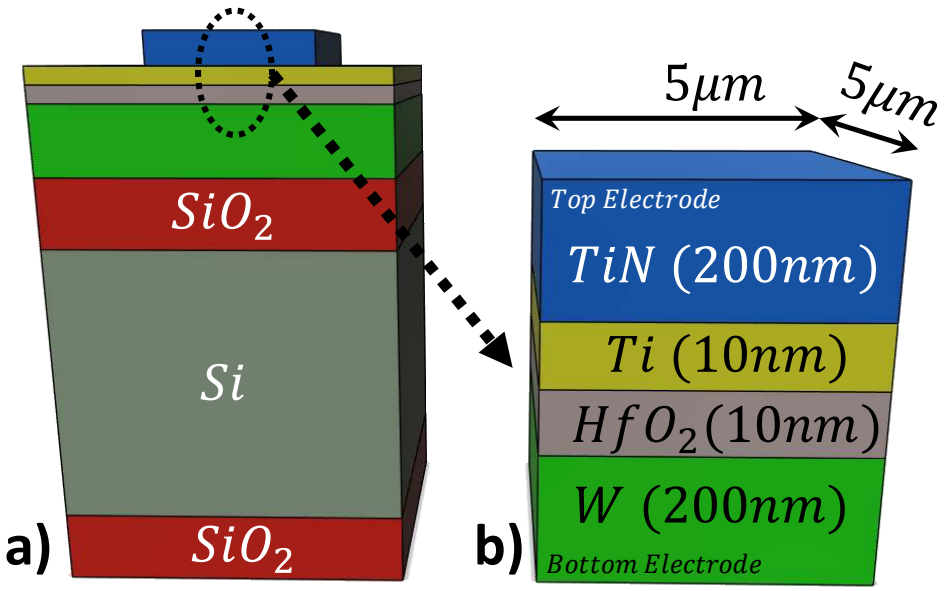

Figure 1. a) Stack structure built on the silicon wafer, b) schematic of the TiN/Ti/HfO_2/W Metal-Insulator-Metal (MIM) RRAM devices.

A particular measurement scheme was used here involving smart control of the compliance current (I_{CC}) of each RS cycle. Ad hoc software was developed for this purpose making use of a Semiconductor Parameter Analyzer (Ag4156C) [1]. The voltage was applied to the top electrode, while the bottom electrode was grounded. After a forming process of I_{cc} = 100μA, a ramped voltage was employed and the negative stop voltage was fixed to -1.6V, to make sure the devices reach the high resistance state (HRS) within the reset process. The smart control of the measurement allows taking decisions during the set process depending on the current, i.e., the voltage will increase until the measured current reaches I_{CC}. At this point the ramped voltage is reversed. In Figure 2a the I-V curves of complete RS cycles are shown for different current compliances. A gradual modification of the compliance current was considered by means of the ramped signal shown in Figure 2b.

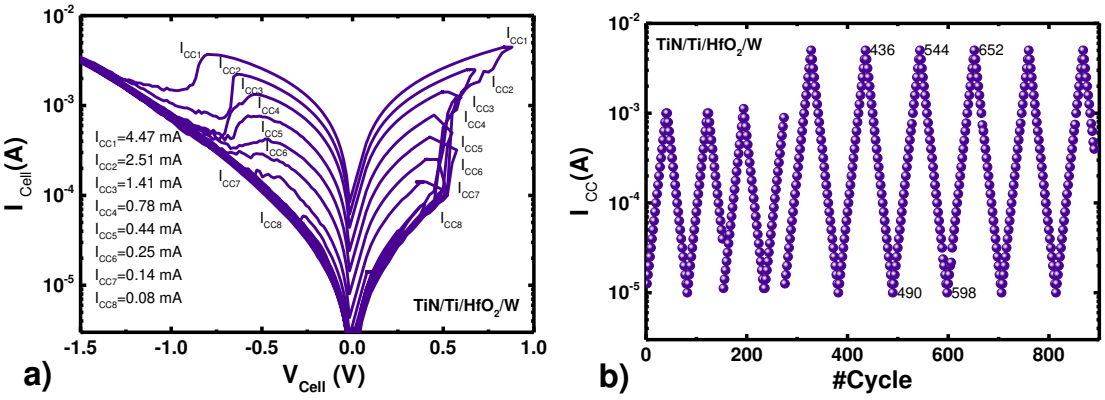

Figure 2. a) I-V curves from RS cycles 545 to 595. The curves were selected in steps of 5 cycles, and they correspond to measurements for different compliance currents. b) I_{CC} variation for the series of 890 RS cycles employed in this manuscript.

As expected, the higher I_{cc} the higher I_{Set} (and I_{Reset}) due to the formation of thicker conductive filaments and correspondingly lower device resistances in the low resistance state (LRS) [4, 5, 14, 15]. A universal trend behind this behavior has been reported previously [16, 17].

III.-PHYSICAL MODEL

The model employed here has been described previously [8, 9] and the devices used in the fitting process reported in [7, 8] are similar. Therefore, the fitting constants reported in the latter references are also used here. The devices are modeled making use of a truncated-cone filament whose shape changes through the RS cycle (reset and set processes) as depicted in Figure 3 [8]. The approach based on the variation of the CF size is in line with previous models found in the literature [5, 12, 13, 17-20]. In this respect, single cylinders [5, 12], truncated-cone-shaped filaments [5, 18] and two cylinder structures in which the smaller cylinder modifies its length and radius [13, 20] and the bigger one is fixed are employed as conductive filaments.

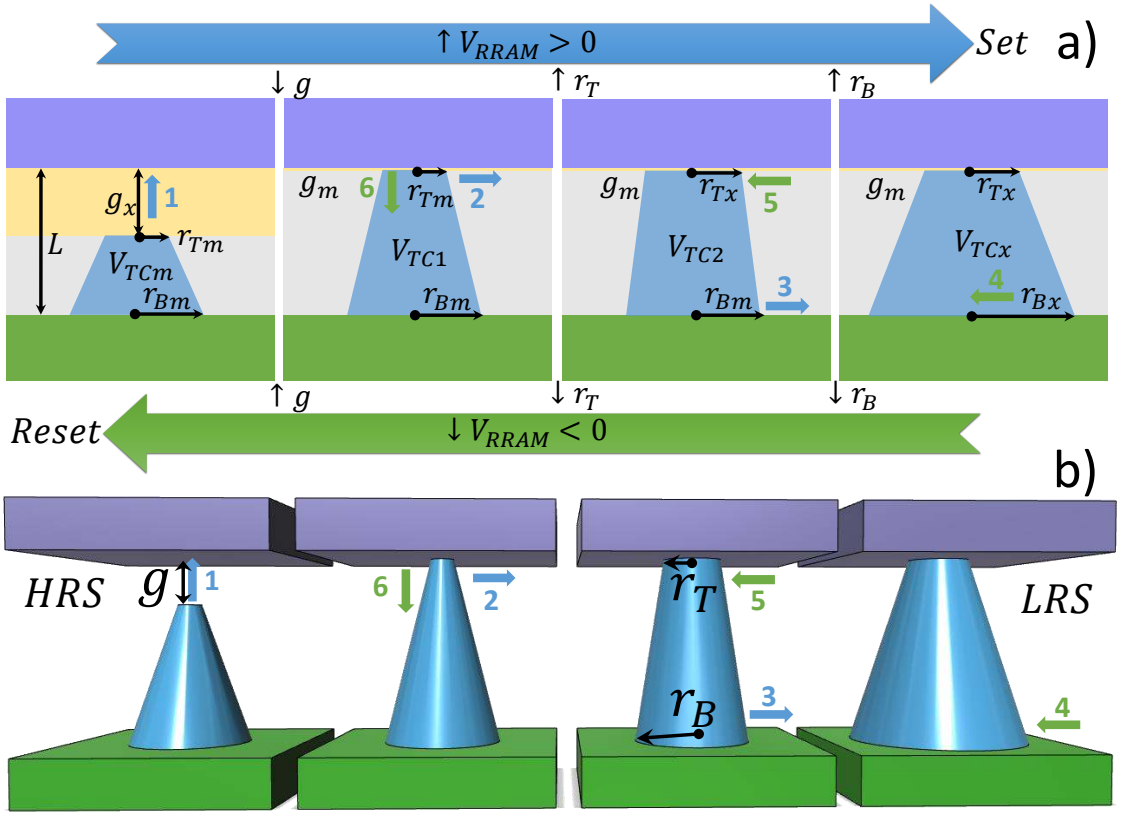

Figure 3. Conductive filament geometry evolution in the model employed to describe RS cycling. The filament volume of the truncated-cone depends on gap (g), the top radius (r_T) and the bottom radius (r_B) that evolve according to equations (1) and (2) following the fixed schema shown in the figure. a) (HRS) Initial CF geometry at its minimum value during the cycle, characterized by a gap length higher than the minimum value (g_m) and close to the maximum (g_x), the minimum top radius (r_{Tm}) and the minimum bottom radius (r_{Bm}). A positive voltage increase leads to a reduction of the gap between the filament tip and the electrode (process 1), until its minimum value, g_m, is reached; if the applied voltage keeps on rising, the CF volume continues its growth by increasing its top radius, r_T (process 2). This parameter is limited by two determined values, $r_{Tm} < r_T < r_{Tx}$. Finally, once r_T reaches its maximum value, it is the bottom radius, r_B, the one that rises till the CF is fully formed (process 3) (the volume reaches its maximum value) and the set process is over. The limits for this radius are the following: $r_{Bm} < r_B < r_{Bx}$. In this case, the LRS is achieved. If the device voltage changes its polarity, the process would lead to a CF volume reduction (a reset process initiates) that would be translated first to a change in r_B, a (process 4) reduction till r_B=r_{Bm}. Later on, a reduction of r_T takes place (process 5) and, finally, a g increase (process 6). At this point, the CF volume reduction is over (the reset process is finished). b) 3D scheme of the CF volume growth (set process, represented by blue arrows, corresponding to positive voltages in Figure 2a) and volume decrease (reset process, represented by green arrows, corresponding to negative voltages in Figure 2a).

The CF geometrical features are shown in Fig 3. We have assumed a truncated-cone shaped CF in line with previous studies involving devices based on Ag/ZrO_2/Pt [21] and Pt/TiO_2/Pt [22] stacks. The CF, with a metallic-like conductivity, is assumed to be made of oxygen vacancies. The migration of oxygen ions, the generation of oxygen vacancies and the

recombination of both species are assumed in simplified the formulation of the Equations 1 and 2, as reported previously [7, 8]. In this work, the evolution of the CF is described by means of Equations 1 and 2 and it is formulated in terms of the CF volume. Taking into consideration the geometrical particularities of our model (Figure 3), we use a three dimensional approximation that allows the description of the truncated-cone shaped CF geometric parameters [23, 24] instead of the variation of the CF radius as was employed in Refs. [5, 12, 25, 26] or the gap between the CF tip and the electrode, as described in Ref. [27].

For the set process, the main physical mechanism that controls the filament evolution is the generation of oxygen vacancies [13, 27]. However, the reset is determined by three processes [13]: electrode release of oxygen ions, movement of the oxygen ions in the oxide layer (via hopping) and recombination between oxygen ions and vacancies. The three processes are also thermally activated. For the sake of simplicity and compactness in the mathematical formulation, we merged in a single equation the previous components [7]. In this respect, we call the reader's attention to the fact that our development falls in the compact modeling approach; an accuracy-simplicity trade-off has been considered since the model is thought to be implemented in simulators to analyze circuits with a very high number of devices.

Therefore, the CF volume temporal evolution is obtained by means of the following equations,

$$\frac{dV_{TC}}{dt} = v_0 \exp\left(-\frac{E_a - \alpha_a Z q \xi}{k_b T}\right) \quad (set) \qquad (1)$$

$$\frac{dV_{TC}}{dt} = -v_0 \exp\left(-\frac{E_r - \alpha_r(g) Z q \xi}{k_b T}\right) \ (reset) \qquad (2)$$

where V_{TC} stands for the CF volume, v_0 for the product of the oxygen ion vibration frequency and the approximated separation between oxygen vacancies, E_a is the average activation energy for oxygen vacancies generation, α_a is the enhancement factor of the electric field, Z is the charge number of oxygen ions, q is the unit charge, ξ is the electric field and k_b is the Boltzmann's constant. The local field strength can be bigger than the average electric field. For this reason, it is usual to employ α_a as a fitting parameter [13], [7]; in addition, it accounts for the polarizability of the dielectric. T is the local temperature obtained by means of the approach detailed in references [7, 8]. In this case the heat equation is solved, and for this purpose a simplifying procedure that considers an equivalent cylinder instead of a truncated-cone shape is employed in order to obtain an analytical expression for the temperature. E_r stands for the average energy that accounts for the aforementioned processes involved in the RESET event. Note that the factor $\alpha_r(g)$, which takes into account the local electric field enhancement depends on the gap because it is expected that the local electric field enhancement in the gap region was bigger than the average electric field as the gap is narrower [27]. For each I-V curve and voltage point, once the CF state has been determined, the current is calculated [7]-[8]. The RRAM equivalent circuit for the current calculation is sketched in Figure 4a. The current sources I_{g1} and I_{g2} correspond to hopping currents through the gap between the filament and the top electrode and from the sides from the filament to the top electrode, respectively. They are

calculated according with expression (19) in [13]. In addition, the top and bottom electrode resistances are represented by R_{CT}, R_{CB}, while R_{CF} is the ohmic resistance due to the formed filament. Finally, R_{ox} and R_g are the resistances linked to the dielectric surrounding the CF and to the dielectric region filling the gap, respectively [7]-[8].

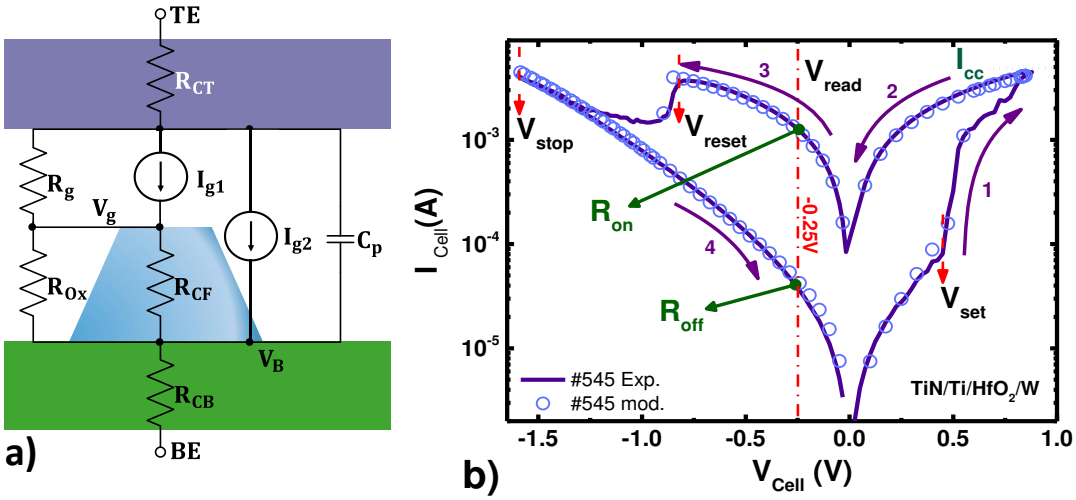

Figure 4. a) Circuit representation of the different electrical components included in the model [7, 8]. b) Description of the I-V curve of a modeled cycle (experimental data are shown in solid lines and modeled data in symbols). Initially, the RRAM is in the HRS. Section 1 of the I-V characteristic and the previous curve region represent a current rise due to a positive ramped voltage applied to the device, a set process takes place when the applied voltage equals V_{Set} (the device enters the LRS). The maximum current is limited by I_{cc}. In section 2, a negative ramped voltage is applied to the RRAM, still with positive voltage values. In section 3, a negative voltage ramp is employed with negative voltages; a final voltage value, V_{Stop}=-1.6V is used. For V_{Cell}=-0.25V (section 3) the R_{on} resistance is measured, and when the voltage reaches V_{Reset} the RRAM changes to the HRS. In section 4, a positive voltage ramp is used increasing voltage values. For V_{Cell}=-0.25V, R_{off} resistance is determined.

IV.-RESULTS AND DISCUSSION

The modeling results for a selected set of experimental I-V curves are shown in Figure 4b and Figure 5 for different I_{CC} values. A good fit is obtained.

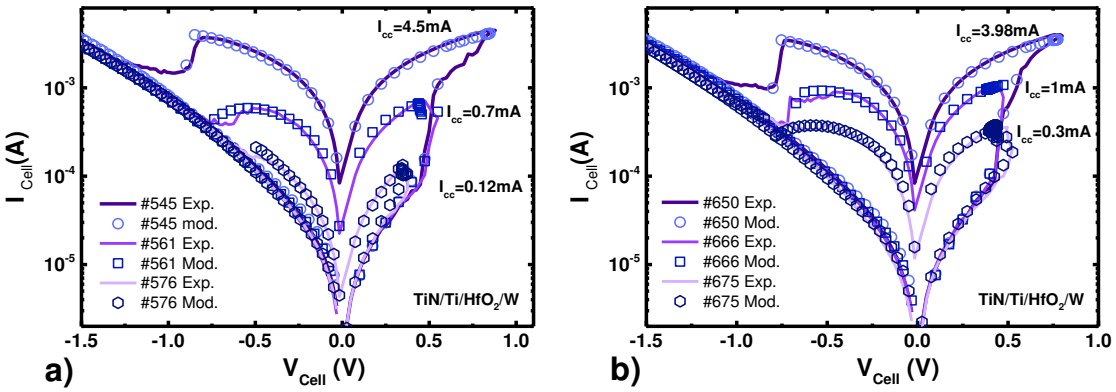

Figure 5. RRAM current versus applied voltage. Experimental data (lines) and modeled data (symbols) are shown for different compliance currents: a) cycle #545 - I_{cc}=4.5mA, cycle #561 - I_{cc}= 0.7mA and cycle #576 - I_{cc}=0.12mA, b) cycle #650 - I_{cc}=3.98mA, cycle #666 - I_{cc}= 1mA and cycle #675 - I_{cc}=0.3mA.

A massive fitting of the 890 RS cycles obtained for the I_{cc} depicted in Figure 2b has been performed. A general framework for the modeling procedure was established by selecting the following geometrical parameters for the truncated-cone shaped CFs: The minimum filament volume is determined by the maximum gap length (g_x=5.4nm) and the minimum top and bottom radii (r_{Tm} =1nm and r_{Bm}=12nm, respectively). The device is in the HRS and during the set process a single oxygen vacancy could close a percolation path, therefore these geometrical values are reasonable. The cycle-to-cycle variability and the different compliance currents used for each cycle lead to different initial and final filament sizes. A different fit was performed for each experimental I-V curve as follows: given an I-V curve, we assume a set of parameters for the model. With these parameters, we obtain (for the same experimental voltages) an array (I_{mod}) of current values provided by

the model for each voltage. Taking into account the Euclidean distance between this array and the array given by the corresponding experimental curves (I_{exp}), the relative error m_I (Equation 3) is determined [28].

$$\boldsymbol{m_I} = \frac{||\boldsymbol{I_{exp}} - \boldsymbol{I_{mod}}||}{||\boldsymbol{I_{exp}}||} \quad (3)$$

where ||…|| represents the norm of the corresponding vector. This value gives us a measure of the error between the experimental and modeled data. A method based on gradient descent algorithm [29] is employed to change the model parameters until a local minimum for m_I is obtained. Figure 6 shows the geometrical parameters corresponding to the state of the filament once the compliance current and maximum positive voltage have been reached. As can be seen, at low compliance currents, the filament barely changes ($g \sim g_x$, $r_T = r_{Tm}$, $r_B = r_{Bm}$).

If the compliance current is higher than 0.055 mA, the filament is allowed to evolve, entering in the tunable region (Figure 6). The higher the compliance current, the lower the final gap length. Once the gap reaches its minimum value, the top radius is allowed to grow to its maximum value and, after that, the bottom radius grows. Therefore, for the cycles where the set process is well completed and the LRS reached, the gap is minimum, the top radii maximum and the bottom radius takes a value between its minimum and maximum values that determines the current in the LRS for each cycle. Note that the CF volume obtained for each I-V curve is different, as expected, and that, because of the scheme we have followed in order to reproduce the CF evolution, the dispersion in the values of the current for completely formed CFs is reflected as a dispersion in the values of the radii,

while a variation in the values of the gap (g) reproduces the dispersion in the values corresponding to the HRS. This result is coherent with the role that I_{cc} plays in limiting the current in each RS cycle and therefore fixing R_{on} value (I_{Reset} is linked to I_{CC} because of this [16]). The region where the gap starts to be reduced is signaled by a vertical dashed line**.** In these cases an operation region with tunable conductivity is entered and RS effects can be employed to mimic synaptic potential in the devices [1, 3] within a neuromorphic circuit context.

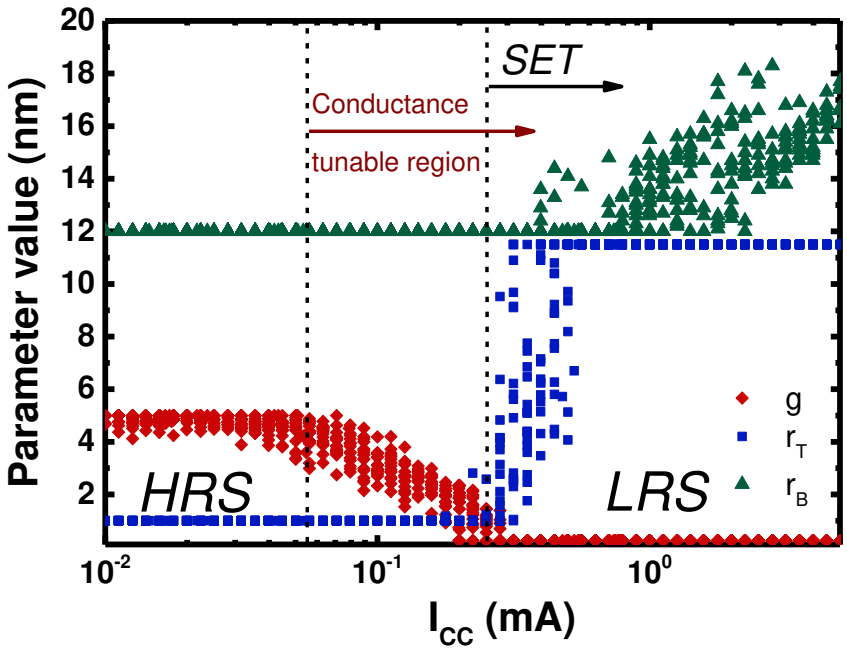

Figure 6: Filament size after the compliance current and the maximum positive voltages are reached (set process), as a function of the compliance current for some of the fitted cycles. The filament final size is given by the gap length (g) and the top and bottom CF radii (r_T and r_B, respectively). In the low I_{CC} region a complete set process is not performed since there is a gap between the CF and the electrode. The tunable region starts when the CF geometry changes (indicated by a dashed line).

A comparison between measured and modeled (after the fitting process) resistances, both in the LRS and HRS, is plotted in Figure 7 to show the goodness of the modeling technique presented for the RS series under study.

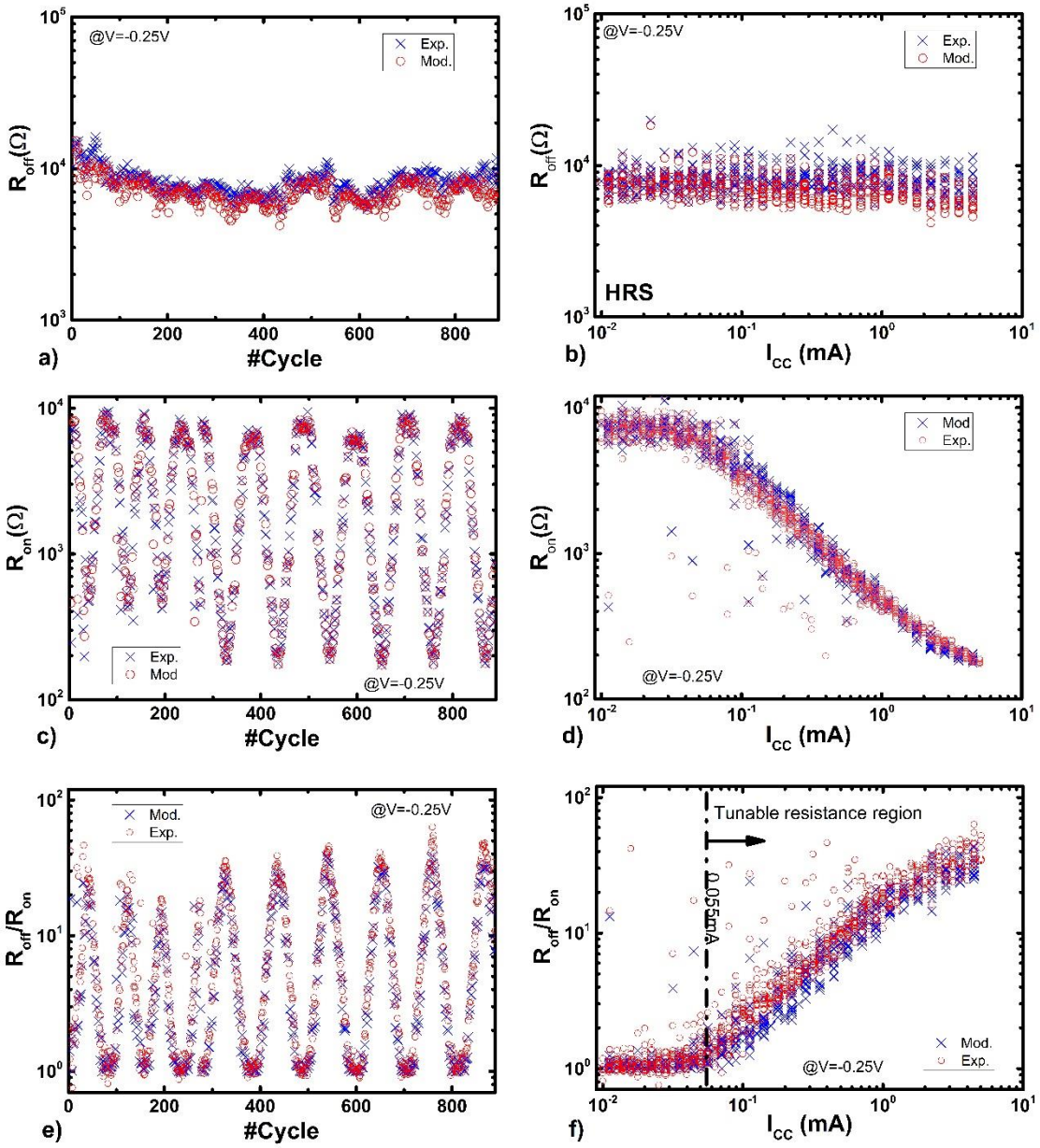

Figure 7. a) R_{off} evolution for the 890 cycles under consideration (measured at V_{Cell}=-0.25V), experimental (modeled) data are shown in blue crosses (red circles), b) R_{off} versus I_{cc} for the cycles considered, c) R_{on} evolution for the 890 cycles under consideration (measured at V_{Cell}=-0.25V), d) R_{on} versus I_{cc}, e) R_{off}/R_{on} ratio versus cycle number, f) R_{off}/R_{on} versus I_{cc}.

A narrow set of R_{off} values is obtained, centered around 10kΩ. The R_{on} value is similar to R_{off} for I_{cc} values below 0.055mA. As highlighted above, it is clear that for these low compliance currents the set process is not performed, therefore R_{on}≈R_{off} (see Figure 7f). The values for parameter *g*

shown in Figure 6 show clearly the non-zero distance from the filament tip to the electrode; in fact, the gap is not modified in these cases. On the contrary, for I_{cc} values higher than 0.055mA, a difference between R_{on} and R_{off} can be seen.

The R_{off}/R_{on} ratio is a measure used by analog circuit designers to determine the level of tuning that the device supports. In our case, this measure shows a two orders of magnitude maximum. Depending on the application, there may be sufficient margin (e.g. to fix weights in neural network implementations). Another issue to highlight here is linked to the possibilities in the realm of multilevel memory circuits.

The histogram and cumulative probability for R_{off} have been shown in Figure 8. It can be seen that the fitting obtained allowed us to reproduce the values accurately.

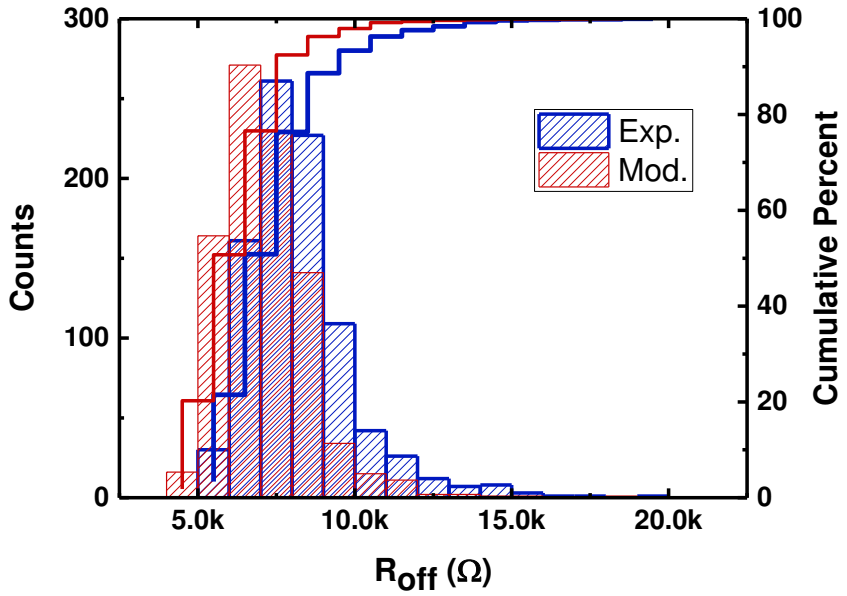

Figure 8. Histogram and cumulative probability for the R_{off} obtained in a set of 890 RS cycles for different I_{cc} values, experimental data (blue) and modeled data (red).

R_{on} versus I_{cc} has been plotted in Figure 9 for modeled and experimental data. The expected values and dependencies are obtained. The plateau observed at low I_{cc} values corresponds to the region where the set process is far from being reached (g remains at its higher value g_x in Figure 6). The on resistance behavior versus the compliance current, $R_{on}(I_{cc})$, can be semiempirically modeled making use of the following analytical expression, with I_{cc} as independent variable,

$$R_{on}(I_{cc}) = \frac{R_o}{1 + \frac{I_{cc}}{I_o}} \quad (4)$$

The paremeter R_o is linked to the HRS resistance (this expression gives a resistance of R_o at low compliance currents). Equation (4) points out how the ratio R_{off}/R_{on} can be modulated by means of the compliance current, I_{CC}. This fact suggests a promising potential for neuromorphic circuit applications taking into consideration the capacity to tune the device conductance (as illustrated by the fitting shown in Figure 9). Comparison of Figures 9a and 9b highlights again the accuracy of the modeling procedure.

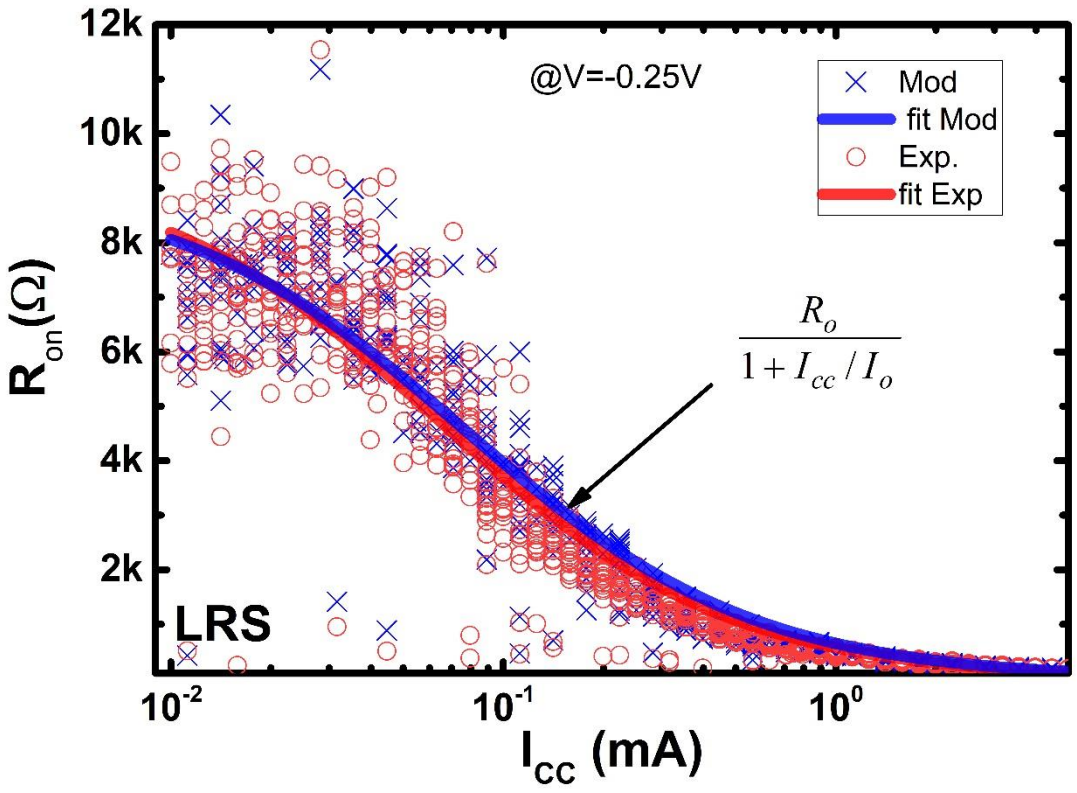

Figure 9. R_{on} versus I_{cc} for the RS series under consideration. Blue crosses and line are used for modeled data, the fitting curve shown (Equation 4) is obtained by means of the following parameters ($R_o = 9461\Omega$, $I_o = 64.41\mu A$); red circles and line are used for experimental data, the fitting curve shown (Equation 4) is obtained making use of the following parameters ($R_o = 9105\Omega$, $I_o = 77.05\mu A$). In both cases the fit reflects 95% confidence bounds.

Note that Expression (4) reduces to the well known relationship R_{on} = $R_o \cdot I_0 / I_{CC}$ [30], for I_{CC} >> I_0. Furthermore, with the values used in this work, the product $R_o \cdot I_0$ is 0.6-0.7V, in the order of V_C = 0.4V in the expression R_{on} = V_C / I_{CC} [20]. In the relation we propose in this work (Expression 4), the parameter I_0 represents a compliance current limit. For compliance currents much lower than this limit, the CF would remain basically unchanged.

As explained above, the CF volume was assumed in Equations 1 and 2 as the variable to be calculated in order to describe RS in the devices under study. The volume reached by the filament after a SET process has been plotted in Figure 10.

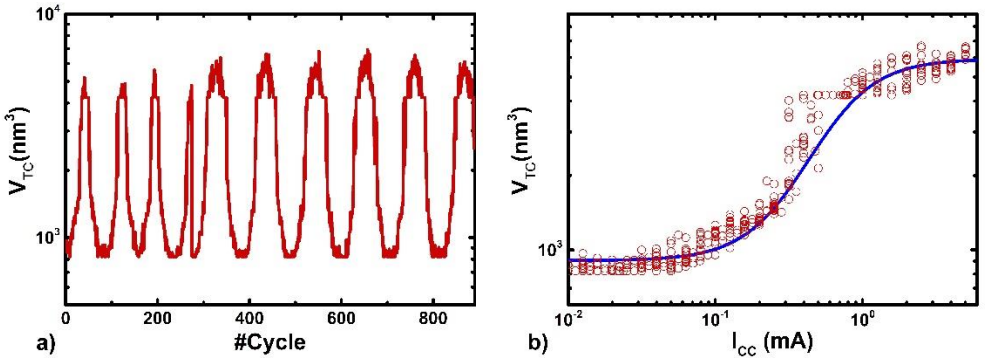

Figure 10: CF volume when the compliance current and the maximum voltage have been reached versus cycle number (a) and versus I_{CC} (b). The shape of the modeled data can be reproduced by a sigmoid function (Equation 5) in a log-log scale. We have performed the fitting with the following parameters (a=8.69, b=6.81, c=14.87 and d=0.52).

See that the CF volume follows the I_{CC} signal employed in the measurement technique, as expected (Figure 10a). The CF volume increases as I_{CC} rises, once a threshold value is reached (the tunable region starts around 0.055 mA, as it can be also seen in Figure 6). This higher volume is reflected in the R_{on} reduction as shown in Figure 9. However, for the highest compliance currents, a certain degree of saturation of the final volume (or resistance) versus compliance current plots appears. That fact is linked to the enhancement of the side components of the current at the highest voltages (modeled by means of I_{g2}, see Figure 4) at the expense of the main current component I_{g1} (which is, therefore, limited by the growing of that side component and that mainly determines the evolution of the filament). This behavior make the shape of the V_{TC}-I_{CC} plot resemble an "S" and, therefore, the distribution of CF volume data shown in Figure 10b can be well fitted with a sigmoid function within a semiempirical approach. In this respect, we have proposed the function given in Equation 5. The fitting is reasonably good, as can be seen in Figure 10b.

$$V_{TC}(I_{CC}) = exp\left(\frac{a-b}{1+exp\left(-\left(\frac{ln(I_{cc})}{d}+c\right)\right)}+b\right) \quad (5)$$

The previous explanation concerning the two hopping currents (I_{g1}, I_{g2}) is coherent with the CF truncated-cone shapes reported in the literature and also with the consideration of other CF shapes, such as tree-branch shapes, where tunneling current components can be found in parallel with ohmic ones due to role played by intermediate oxygen vacant clusters close to the percolation paths.

It has been highlighted that when small variation of the compliance current is employed, a better control of the device resistance is achieved in comparison with random variations of the compliance current [1]. A coherent explanation of this effect can be given in the context of RS Kinetic Monte Carlo simulation [4, 11, 31-34]. It is seen that reduction (oxidation) activation energies of ion (atoms) within the dielectric that contribute to the percolation paths and configure the CFs depend on the number of atoms surrounding them [4, 31]. Therefore, the cluster formation, that constitutes the first stage in percolation path evolution, can be favored if small variations of I_{CC} are employed in a cycle-to-cycle basis. In this manner, better control of the density of defects in the CF is achieved and consequently the device conductivity can be modulated more easily. It was also addressed the issue connected to the different manners of defining the end of reset processes [1]. One of them fixing a stop voltage allows better control of R_{off}; while other processes, which are stopped when a current drop is detected, does not allow control of R_{off}. This effect can be explained

if we concentrate our reasoning on the parameter *g* in our model (the gap distance, see Figure 3). In this respect, the current drop is produced by the sudden increase of the gap between the filament tip and the electrode. Since the device current depends exponentially on *g* [8], we would find out different gaps if the reset process is stopped when the device current drops off. Consequently, different gaps could be formed and very different currents (since the current depends exponentially on the gap distance) would be obtained, this could lead to a great R_{off} variability.

Finally, we can assess the maximum temperature obtained in the set process for each of the I_{CC} modeled. It has been plotted in Figure 11. The temperature was obtained by solving the 1D heat equation considering a cylindrical shaped CF. We include a term weighted by a heat transfer coefficient to account for the lateral heat dissipation from the CF to the dielectric. The Joule heating was calculated by means of the electrical conductivity and the electric field in the CF. More details are given in Ref. 8.

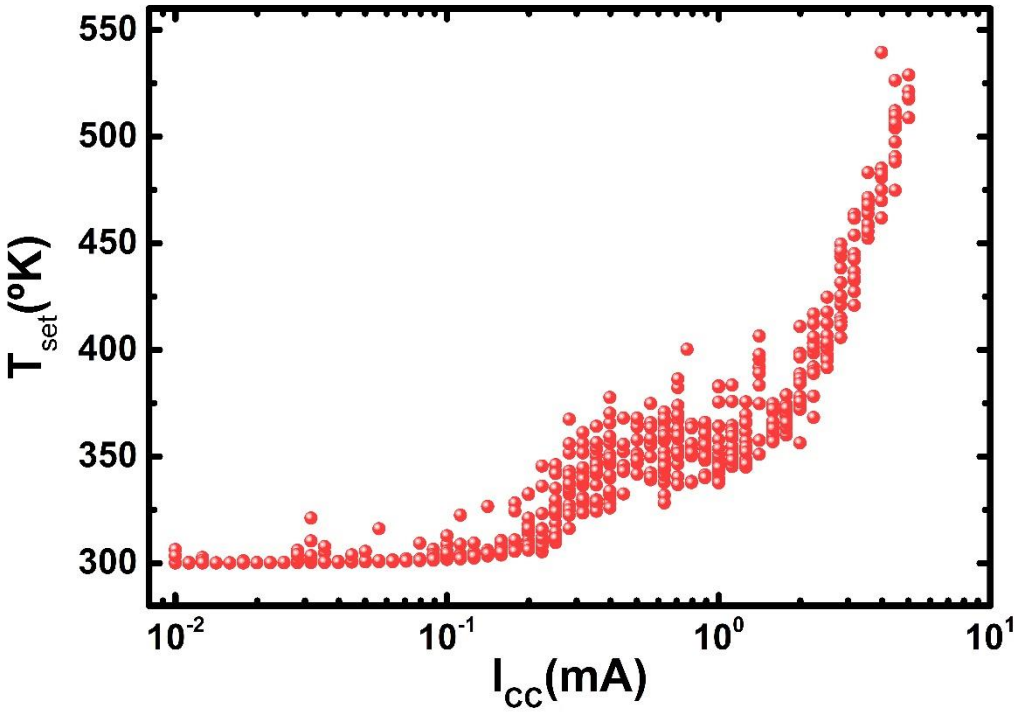

Figure 11. Maximum temperature in the set process versus compliance current.

As expected, at low compliance currents the temperature does not increase due to the lower currents achieved and the low Joule heating effects. However, once the gap parameter achieves its minimum value, the current, heating effects and CF temperature go up.

V.-CONCLUSIONS

A physical compact model to analyze electronic synapses based on resistive switching devices has been employed to describe the influence of the compliance current on the resistive switching processes. The modelling approach makes use of truncated-cone shaped CF geometries and parasitic ohmic resistances. A new measurement procedure was employed to gradually change the compliance current. The analysis consisted of a

massive fitting of 890 RS cycles to understand the effects of compliance current variation. An in-depth comparison between measured and modeled data was performed to show the accuracy of the modeling technique in reproducing a modulation ratio of the resistance and the compliance current in two decades. Therefore, the results helped to clarify the devices potential to work as synaptic elements in neuromorphic circuits taking into consideration the conductivity gradual control capacity observed. As shown, this compact modeling approach could be used to aid neuromorphic circuit designers by allowing simulations at a circuit level.

VI. - ACKNOWLEDGMENTS

The authors thank the support of the Spanish Ministry of Economy, Industry and Competitiveness under projects TEC2017-84321-C4-1-R, TEC2017-84321-C4-3-R, TEC2014-54906-JIN and TEC2016-75151-C3-1-R (also supported by the FEDER program). This work has made use of the Spanish ICTS Network MICRONANOFABS.

References

[1] M. Pedro, J. Martin-Martinez, M.B. Gonzalez, R. Rodriguez, F. Campabadal, M. Nafria, Xavier Aymerich, "Tuning the conductivity of resistive switching devices for electronic synapses", Microelectronic Engineering, Vol. 178, pp. 89-92, 2017.

[2] S. Yu, Y. Wu, R. Jeyasingh, D. Kuzum, H.-S. Wong, "An electronic synapse device based on metal oxide resistive switching memory for neuromorphic computation", IEEE Trans. Electron Devices, 58 (8), pp. 2729–2737, 2011. DOI: 10.1109/TED.2011.2147791.

[3] S. Yu, "Neuro-inspired computing using resistive synaptic devices", Springer, 2017. ISBN: 978-3-319-54312-3

[4] F. Pan, S. Gao, C. Chen, C. Song, F. Zeng, "Recent progress in resistive random access memories: materials, switching mechanisms and performance", Materials Science and Engineering, 83, pp. 1-59, 2014. DOI: 10.1016/j.mser.2014.06.002

[5] M.A. Villena, J.B. Roldán, F. Jiménez-Molinos, E. Miranda, J. Suñé, M. Lanza, "SIM^{2}RRAM: a physical model for RRAM devices simulation", Journal of Computational Electronics, 2017. DOI: 10.1007/s10825-017-1074-8

[6] N. Suri, "Advances in neuromorphic hardware exploiting emergin nanoscale devices", Springer, 2017. DOI:10.1007/978-81-322-3703-7

[7] G. González-Cordero, F. Jiménez-Molinos, J.B. Roldan, M.B. González and F. Campabadal, "In-depth study of the physics behind resistive switching in TiN/Ti/HfO2/W structures". J. Vac. Sci. Technol. B 35, 01A110, 2017 DOI: 10.1116/1.4973372.

[8] G. González-Cordero, M.B. González, H. García, F. Campabadal, S. Dueñas, H. Castán, F. Jiménez-Molinos, J.B. Roldán, "A physically based model for resistive memories including a detailed temperature and variability description", Microelectronic Engineering, Vol. 178, pp. 26-29, 2017. DOI: 10.1016/j.mee.2017.04.019

[9] G. González-Cordero, M. B. González, H. García, F. Jiménez-Molinos, F. Campabadal, S. Dueñas, H. Castán and J. B. Roldán, "A Physically Based Model to describe Resistive Switching in different RRAM technologies", in 11th edition of the Spanish Conference on Electron Devices (CDE), in Barcelona, Spain, 2017. DOI: 10.1109/CDE.2017.7905223

[10] M.A. Villena, J.B. Roldán, M.B. González, P. González-Rodelas, F. Jiménez-Molinos, F. Campabadal, D. Barrera, "A new parameter to characterize the charge transport regime in Ni/HfO_2/Si-n^+-based RRAMs", Solid State Electronics, vol. 118, pp. 56-60, 2016. DOI: 10.1007/s10825-017-1074-8

[11] A. Padovani, L. Larcher, O. Pirrotta, L. Vandelli and G. Bersuker, "Microscopic Modeling of HfOx RRAM Operations: From Forming to Switching", IEEE Transactions on Electron Devices, 62(6), pp. 1998-2006, 2015. DOI: 10.1109/TED.2015.2418114

[12] M. Bocquet, D. Deleruyelle, H. Aziza, C. Muller, J. Portal, T. Cabout, E. Jalaguier, "Robust compact model for bipolar oxide-based resistive switching memories", IEEE Transactions on Electron Devices, 61, pp. 674-681, 2014. DOI: 10.1109/FTFC.2013.6577779

[13] P. Huang, X. Y. Liu, B. Chen, H.T. Li, Y. J. Wang, Y.X. Deng, K.L. Wei, L. Zeng, B. Gao, G. Du, X. Zhang, J.F. Kang, "A Physics-Based Compact Model of Metal-Oxide-Based RRAM DC and AC Operations," Electron Devices, IEEE Transactions on, vol.60, no.12, pp. 4090-4097, 2013. DOI: 10.1109/TED.2013.2287755

[14] M. Lanza, "A Review on Resistive Switching in High-k Dielectrics: A Nanoscale point of View Using Conductive Atomic Force Microscope", Materials 7, pp. 2155-2182, 2014. DOI: 10.3390/ma7032155.

[15] M.A. Villena, M.B. González, F. Jiménez-Molinos, F. Campabadal, J.B. Roldán, J. Suñé, E. Romera, E. Miranda, "Simulation of thermal reset transitions in RRAMs including quantum effects", Journal of Applied Physics, vol. 115, pp. 214504, 2014. DOI: 10.1063/1.4881500

[16] D. Ielmini, R. Waser. "Resistive Switching: From Fundamentals of Nanoionic Redox Processes to Memristive Device Applications", Wiley-VCH, 2015. DOI: 10.1002/9783527680870

[17] F. Nardi, S. Larentis, S. Balatti, D. C. Gilmer, and D. Ielmini, "Resistive Switching by Voltage-Driven Ion Migration in Bipolar RRAM—Part I: Experimental Study", IEEE Trans. Elec. Dev., vol 59, p. 2461, 2012. DOI: 10.1109/TED.2012.2202319

[18] G. Gonzalez-Cordero, J. B. Roldan, F. Jimenez-Molinos, J. Suñé, S. Long and M. Liu, "A new compact model for bipolar RRAMs based on truncated cone conductive filaments, a Verilog-A approach," Semicond. Sci. Technol., vol. 31, no. 11, pp. 1–13, 2016. DOI: 10.1088/0268-1242/31/11/115013

[19] F. Jiménez-Molinos, M.A. Villena, J.B. Roldán, A.M. Roldán, "A Spice Compact Model For Unipolar RRAM Reset Process Analysis", IEEE Trans. Elec. Dev., vol 62, pp. 955-962, 2015. DOI: 10.1109/TED.2014.2387429

[20] D. Ielmini, "Modeling the Universal Set/Reset Characteristics of Bipolar RRAM by Field- and Temperature-Driven Filament Growth", IEEE Transactions on Electron Devices, vol 58, no. 12, pp. 4309-4317, 2011.

[21] J. Sun, X. Wu, Q. Liu, M. Liu, L.T. Sun, "Real time observation of nanoscale multiple conductive filaments in RRAM by using advanced in-situ TEM", 2013 20th IEEE International Symposium on the Physical and Failure Analysis of Integrated Circuits (IPFA), pp. 560–562, 2013. DOI: 10.1109/IPFA.2013.6599223

[22] D.-H. Kwon, K. M. Kim, J. H. Jang, J. M. Jeon, M. H. Lee, G. H. Kim, X.-S. Li, G.-S. Park, B. Lee, S. Han, M. Kim, and C. S. Hwang, "Atomic structure of conducting nanofilaments in TiO2 resistive switching memory," Nat. Nanotechnol., vol. 5, no. 2, pp. 148–153, Feb. 2010. DOI: 10.1038/nnano.2009.456

[23] K.M. Kim, C.S. Hwang, "The conical shape filament growth model in unipolar resistance switching of TiO2 thin film", Applied Physics Letters, 94(12), PP. 10–13, 2009. DOI: 10.1063/1.3108088.

[24] K.M. Kim, M.H. Lee, G.H. Kim, S.J. Song, J.Y. Seok, J.H. Yoon, C.S. Hwang, "Understanding structure-property relationship of resistive switching oxide thin films using a conical filament model", Applied Physics Letters, 97(16), 2010. DOI: 10.1063/1.3505354

[25] M.A. Villena, M.B. González, J.B. Roldán, F. Campabadal, F. Jiménez-Molinos, F.M. Gómez-Campos y J. Suñé, "An in-depth study of thermal effects in reset transitions in HfO2 based RRAMs", Solid State Electronics, 111, pp. 47-51, 2015. DOI: 10.1016/j.sse.2015.04.008.

[26] M. Bocquet, D. Deleruyelle, C. Muller, J.M. Portal, "Self-consistent physical modeling of set/reset operations in unipolar resistive-switching memories". *Applied Physics Letters*, *98*, p. 263507, 2011. DOI: 10.1063/1.3605591

[27] Guan, Ximeng, Shimeng Yu, and H-S. Philip Wong. "A SPICE compact model of metal oxide resistive switching memory with variations." IEEE electron device letters 33.10, pp. 1405-1407, 2012. DOI: 10.1109/LED.2012.2210856

[28] S. Kvatinsky, M. Ramadan, E. G. Friedman and A. Kolodny, "VTEAM: A General Model for Voltage-Controlled Memristors," in IEEE Transactions on Circuits and Systems II: Express Briefs, vol. 62, no. 8, pp. 786-790, Aug. 2015. DOI: 10.1109/TCSII.2015.2433536

[29] R.W. Cottle, M.N. Thapa, "Descent methods. In Linear and Nonlinear Optimization", (1st ed., pp. 317–368). New York: Springer-Verlag, 2017. DOI: 10.1007/978-1-4939-7055-1_10

[30] S. Kim, C. Du, P. Sheridan, W. Ma, S. Choi, W. D. Lu, "Experimental Demonstration of a Second-Order Memristor and Its Ability to Biorealistically Implement Synaptic Plasticity" *Nano Lett. 15*, 2203, 2015.

[31] S. Aldana, P. García-Fernández, A. Rodríguez-Fernández, R. Romero-Zaliz, M.B. González, F. Jiménez-Molinos, F. Campabadal, F. Gómez-Campos, J.B. Roldán, "A 3D Kinetic Monte Carlo simulation study of Resistive Switching processes in Ni/HfO2/Si-n+-based RRAMs", Journal of Physics D: Applied Physics, 50, 335103, 2017. DOI: 10.1088/1361-6463/aa7939

[32] X. Guan, S. Yu and H.-P. Wong, "On the switching parameter variation of metal-oxide RRAM—Part I: Physical modeling and simulation methodology", *IEEE Transactions on Electron Devices,* 59, pp. 1172-1182, 2012. DOI: 0.1109/TED.2012.2184545

[33] S. Yu, X. Guan, H.S. Philip Wong, "On the switching parameter variation of metal oxide RRAM—Part II: Model corroboration and device design strategy", IEEE Transactions on Electron Devices, 59, pp. 1183-1188, 2012. DOI: 10.1109/TED.2012.2184544

[34] J. Guy, G. Molas, P. Blaise, M. Bernard, A. Roule, G. Le Carval, V. Delaye, A. Toffoli, G. Ghibaudo, *Fellow, IEEE*, F. Clermidy, B. De Salvo, L. Perniola , "Investigation of Forming, SET, and Data Retention of Conductive-Bridge Random-Access Memory for Stack Optimization", IEEE Transactions on Electron Devices, *62*(11), pp. 3482-3489, 2015. DOI: 10.1109/TED.2015.2476825